

Actively tunable polarization-sensitive multiband absorber based on graphene

Ai-Li Cao(曹爱利), Kun Zhang(张昆), Jia-Rui Zhang(张佳瑞), Yan Liu(刘燕), Wei-Jin Kong(孔伟金)

Citation: Chin. Phys. B . 2020, 29(11): 114205 . **doi:** 10.1088/1674-1056/abb663
Journal homepage: http://cpb.iphy.ac.cn; http://iopscience.iop.org/cpb

What follows is a list of articles you may be interested in

Polarization-insensitive complementary metamaterial structure based on graphene for independently tuning multiple transparency windows

Hailong Huang(黄海龙), Hui Xia(夏辉), Hongjian Li(李宏建)

Chin. Phys. B . 2020, 29(11): 114203 . **doi:** 10.1088/1674-1056/abb307

An improved method for the investigation of high-order harmonic generation from graphene

Zhong Guan(管仲), Lu Liu(刘璐), Guo-Li Wang(王国利), Song-Feng Zhao(赵松峰), Zhi-Hong Jiao(焦志宏), Xiao-Xin Zhou(周效信)

Chin. Phys. B . 2020, 29(10): 104206 . **doi:** 10.1088/1674-1056/abab76

An ultrafast and low-power slow light tuning mechanism for compact aperture-coupled disk resonators

Bo-Yun Wang(王波云), Yue-Hong Zhu(朱月红), Jing Zhang(张静), Qing-Dong Zeng(曾庆栋), Jun Du(杜君), Tao Wang(王涛), Hua-Qing Yu(余华清)

Chin. Phys. B . 2020, 29(8): 084211 . **doi:** 10.1088/1674-1056/ab9df1

Low-power electro-optic phase modulator based on multilayer graphene/silicon nitride waveguide

Lanting Ji(姬兰婷), Wei Chen(陈威), Yang Gao(高阳), Yan Xu(许言), Chi Wu(吴锜), Xibin Wang(王希斌), Yunji Yi(衣云骥), Baohua Li(李宝华), Xiaoqiang Sun(孙小强), Daming Zhang(张大明)

Chin. Phys. B . 2020, 29(8): 084207 . **doi:** 10.1088/1674-1056/ab943b

A compact electro-absorption modulator based on graphene photonic crystal fiber

Guangwei Fu(付广伟), Ying Wang(王颖), Bilin Wang(王碧霖), Kaili Yang(杨凯丽), Xiaoyu Wang(王晓愚), Xinghu Fu(付兴虎), Wa Jin(金娃), Weihong Bi(毕卫红)

Chin. Phys. B . 2020, 29(3): 034209 . **doi:** 10.1088/1674-1056/ab6838

Actively tunable polarization-sensitive multiband absorber based on graphene*

Ai-Li Cao(曹爱利), Kun Zhang(张昆)†, Jia-Rui Zhang(张佳瑞), Yan Liu(刘燕), and Wei-Jin Kong(孔伟金)‡

College of Physics Science, Center for Marine Observation and Communications, Qingdao University, Qingdao 266071, *China*

(Received 3 July 2020; revised manuscript received 12 August 2020; accepted manuscript online 9 September 2020)

We design an actively tunable polarization-sensitive multiband absorber in the mid-infrared region, which consists of stacked graphene multilayers separated by dielectric layers on a metal mirror. Benefiting from the anisotropic structure, the absorber has dual absorption bands with almost perfect absorption at different wavelengths under the *x* and *y* polarizations. Analyzing the electric field amplitude distributions and the surface currents, we find that the absorption peaks under the same polarization are excited in the graphene layers independently. Therefore, more absorption bands can be achieved by increasing the graphene layers. Adjusting the Fermi energy of the graphene layers, the working wavelengths of the polarization-sensitive multiband absorbers can be tuned actively, and thus achieving a wide band regulation range. Besides, the peak number and the peak strength of the multiband absorber can be actively controlled by the polarization angle as well. We also propose a method to design an actively tunable polarization-sensitive multiband absorber, which may have potential applications in mid-infrared devices, such as polarization-sensitive filters and detectors.

Keywords: multiband absorber, polarization-sensitive, graphene, band regulation

PACS: 42.25.Ja, 42.25.Bs **DOI:** 10.1088/1674-1056/abb663

1. Introduction

Metamaterial is an artificial composite material that does not exist in nature and has interesting electromagnetic properties.[1–4] As a crucial component of metamaterial, metamaterial absorber[5] has caused widespread concern, in which the reflection is suppressed by matching the impedance of the metamaterial with the impedance of the incident medium, while the transmission is suppressed by adding a metal-based layer to achieve perfect absorption.[6] In 2008, Landy *et al.* proposed a metamaterial perfect absorber experimentally and theoretically.[7] Since then, various absorbers have been constantly innovated by employing periodic array structures in a band from visible light to terahertz,[8–12] achieving narrow band and broadband absorption.

Due to the excellent optical and electrical properties, graphene has been one of the most popular candidates to introduce active regulation method into metamaterials over the past decade.[13–16] In terms of light absorption, graphene has greater advantages in the band from mid-infrared to terahertz than in the visible near infrared band Up to now, circular,[17,18] square,[19] cross,[20] square ring,[21] and other isotropic structures have been employed to design polarization-independent absorbers based on graphene, realizing narrowband, multiband[22–25] and even broadband[26] absorption. On the other hand, polarization-sensitive absorbers have been proposed by employing anisotropic units.[27,28] However, most of the polarization-sensitive absorbers based on graphene are single-band and broadband absorbers.[29]

In this paper, we design an actively tunable polarization-sensitive multiband absorber in the mid-infrared region, based on the stacked graphene multilayers. Inspired by the work proposed by Bao *et al.*,[21] we take advantage of the anisotropic structure with a circle hole to enhance the absorption which shows that the multi-band absorption is sensitive to the polarization of incident light. In simulation, the designed structure can achieve dual-band absorption over 90% at different wavelengths under different polarizations. Adjusting the Fermi energy of the graphene layer, the absorption band can realize the dynamic regulation of extremely wide band. Moreover, changing the incident polarization angle, tunable multiband absorption can be realized as well. In our work we propose a method to design an actively tunable polarization-sensitive multiband absorber, which may achieve potential applications in mid-infrared integrated devices.

2. Structure design

The unit of the designed absorber is schematically shown in Fig. 1, which consists of two graphene patches separated by a silica layer. The double-layer graphene patch placed on the silica layer is over a thick gold mirror. The surface current formed between the aperture and the graphene rectangle can relatively enhance the absorption. In simulation, the refractive index of the silica material is set to be 1.45.[30] Drude model is used to calculate the permittivity of gold ($\varepsilon(\omega)$) from the

*Project supported by the National Natural Science Foundation of China (Grant Nos. 11804178 and 11274188) and the Natural Science Foundation of Shandong Province, China (Grant No. ZR2018BA027).

†Corresponding author. E-mail: zkun@qdu.edu.cn

‡Corresponding author. E-mail: kwjsd@163.com

© 2020 Chinese Physical Society and IOP Publishing Ltd

following equation:

$$\varepsilon(\omega)=1-\frac{\omega_{\mathrm{p}}^2}{\omega^2+\mathrm{i}\omega\gamma}, \tag{1}$$

where ω is the source frequency, ω_{p} is the plasma frequency and $\omega_{\mathrm{p}}=8.67\times10^{16}$ rad/s, γ is the collision frequency, and $\gamma=7.72\times10^{14}$ rad/s.[31] The surface conductivity of graphene is calculated based on the Kubo formula[32–34]

$$\begin{aligned}\sigma = \sigma_{\mathrm{inter}}+\sigma_{\mathrm{intra}} = &\frac{2e^2k_{\mathrm{B}}T}{\pi\hbar^2}\frac{\mathrm{i}}{\omega+\mathrm{i}\tau^{-1}}\ln\left[2\cosh\left(\frac{E_{\mathrm{F}}}{2k_{\mathrm{B}}T}\right)\right]\\ &+\frac{e^2}{4\hbar}\left[\frac{1}{2}+\frac{1}{\pi}\arctan\left(\frac{\hbar\omega-2E_{\mathrm{F}}}{2k_{\mathrm{B}}T}\right)\right]\\ &-\frac{e^2}{4\hbar}\left[\frac{\mathrm{i}}{2\pi}\ln\frac{(\hbar\omega+2E_{\mathrm{F}})^2}{(\hbar\omega-2E_{\mathrm{F}})^2+4(k_{\mathrm{B}}T)^2}\right],\end{aligned} \tag{2}$$

where T is the temperature, k_{B}, $\hbar$ E_{F}, τ and e are the Boltzmann constant, reduced Planck constant, Fermi energy momentum relaxation time, and electron charge, respectively. When graphene is highly doped with $E_{\mathrm{F}}\gg k_{\mathrm{B}}T$ and $E_{\mathrm{F}}\gg\hbar\omega$, equation (2) can be simplified into[35,36]

$$\sigma=\frac{e^2E_{\mathrm{F}}}{\pi\hbar^2}\frac{\mathrm{i}}{\omega+\mathrm{i}\tau^{-1}}, \tag{3}$$

where $\tau=\mu E_{\mathrm{F}}/(ev_{\mathrm{F}}^2)$, the carrier mobility $\mu=1\times10^4$ cm^2/(V·s), and Fermi velocity $v_{\mathrm{F}}=1\times10^6$ m/s, respectively.[37] The expression between Fermi energy and bias voltage V_{g} is given by $E_{\mathrm{F}}\approx\hbar v_{\mathrm{F}}\sqrt{\pi\varepsilon_0\varepsilon_{\mathrm{r}}V_{\mathrm{g}}/ed}$,[38] where d is the thickness of the gate silica layer, ε_{r} and ε are the permittivity of the silica and vacuum, respectively. Therefore, the Fermi level can be controlled experimentally by the bias voltage V_{g}.

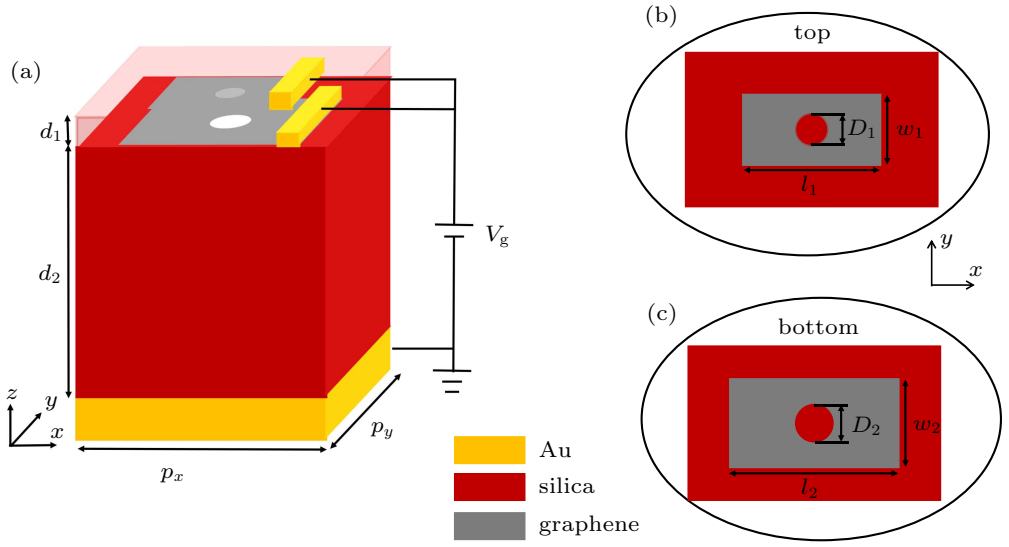


Fig. 1. (a) Schematic diagram of graphene-based absorber. Top view of (b) top and (c) bottom graphene patches.

We employ the finite-difference time-domain (FDTD) method to optimize the geometric parameters when fixing E_{F} at 0.65 eV. As shown in Fig. 1(a), the boundary condition in the z direction perfectly matches the layer (PML), while those in x and y direction are periodic with period $p_x=800$ nm and $p_y=700$ nm. The geometric parameters of the top graphene patch are $l_1=500$ nm, $w_1=250$ nm, and $D_1=112$ nm as shown in Fig. 1(b), and those of the bottom graphene patch are $l_2=600$ nm, $w_2=360$ nm, and $D_2=110$ nm as shown in Fig. 1(c). The thickness values of the dielectric layers are $d_1=350$ nm and $d_2=1700$ nm, respectively. The top silica is used to weaken the coupling of two layers of graphene. The bottom silica helps match the effective impedance of the structure with that of free space, leading to the perfect absorption.[17]

In the practical sample fabrication, Au and silica can be successively deposited on the silicon substrate by electron beam evaporation, and then the graphene sheet grown by chemical vapor deposition can be transferred onto silica. The graphene structure can be fabricated by e-beam lithography followed by plasma etching.[28] Finally, the gold electrode can be deposited by electron beam evaporation. Repeating the above steps, the bi-layer graphene absorber can be obtained.

3. Results and discussion

In order to illustrate the anisotropic absorption principles of the graphene-based structure, we calculate the absorption spectra under the x and y polarized incidences, as plotted in Fig. 2. For the x polarization in Fig. 2(a), there are two absorption peaks (P_1 and P_2) higher than 90% those at the wavelengths 27.3 μm and 31.9 μm. For the y polarization in Fig. 2(b), the two absorption peaks (P_3 and P_4) can also reach higher than 90% at the wavelengths 16.3 μm and 21.2 μm. Therefore, polarization-sensitive absorption is realized in this structure. For comparison, we calculate the absorption spectra of the structure containing only the top graphene patch (red dashed line) or only the bottom graphene patch (blue dashed

line) as shown in Figs. 2(a) and 2(b). It is obvious that there is a weak coupling between the absorption modes excited at the top and the bottom graphene patches, leading the peaks to slightly shift. As a result, the overall absorption spectra in Fig. 2 are almost the combination of those of the top and bottom graphene patches.

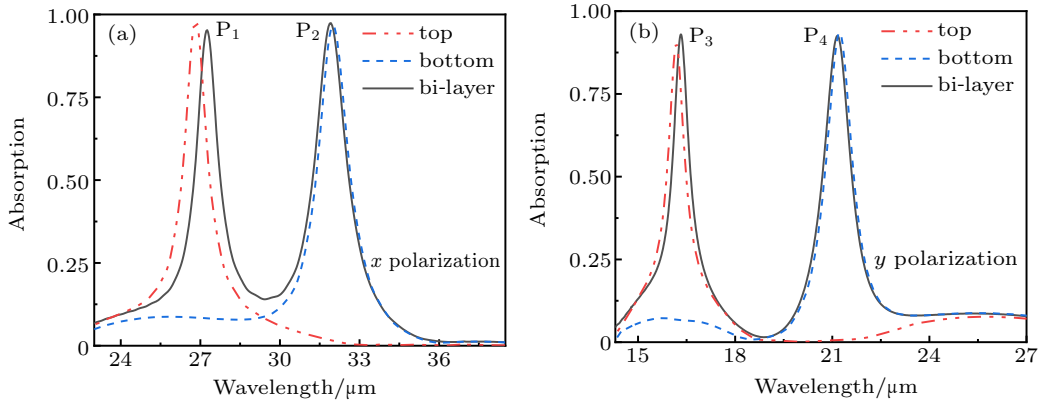


Fig. 2. Absorption spectra under (a) *x*- and (b) *y*-polarized incident light with black solid line, red dashed line, and blue dashed line denoting structures including dual-layer graphene patches, top graphene patch, and bottom graphene patch, respectively.

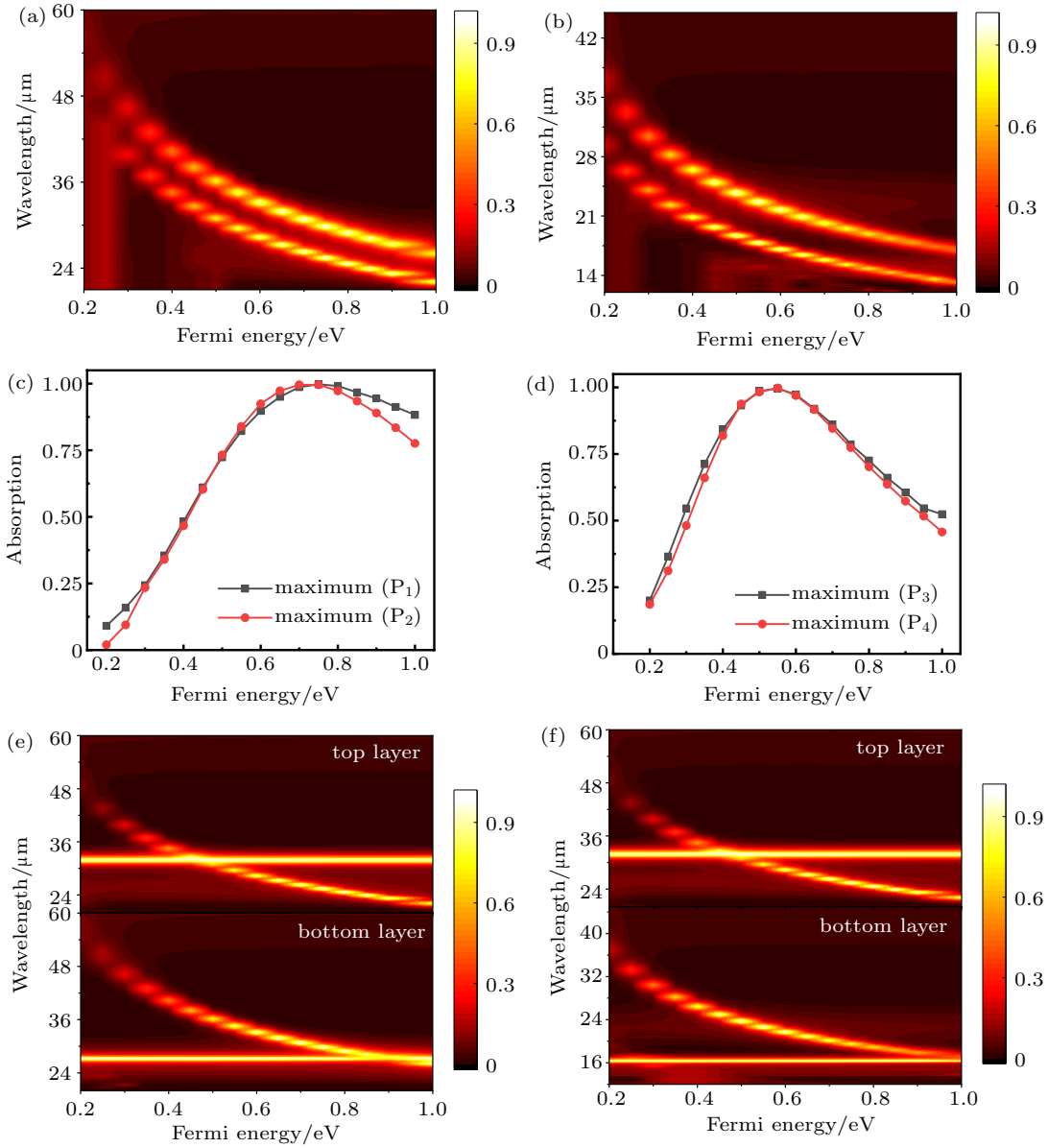


Fig. 3. Absorption spectra for different values of E_F under (a) *x* polarization and (b) *y* polarization, respectively, relationship between the maximum absorption intensity and E_F under (c) *x* polarization and (d) *y* polarization, and [(e) and (f)] absorption spectra for changing E_F of each graphene layer individually under *x* and *y* polarizations.

The Fermi energy E_F of the graphene can actively tune the absorption spectrum byusing the surface conductivity. We simultaneously tune the E_F values of the two graphene layers to explore the influence. As shown in Figs. 3(a) and 3(b), the absorption peaks all have blue-shifts with E_F increasing. It is obvious that the wavelengths of the peaks under the same polarization vary at an identical dispersion rate. Figures 3(c) and 3(d) show the changes of maximum absorption under the x and y polarizations, respectively. The absorption intensities both first increase and then decrease with the increase of E_F, reaching nearly perfect absorption at $E_F = 0.75$ eV under the x polarization, and at 0.55 eV under the y polarization. Besides, as the coupling between the top graphene and bottom graphene is weak, the peaks can be independently controlled by regulating the E_F of each graphene layer respectively as shown in Figs. 3(e) and 3(f). The peaks related to the regulated graphene layer have the same changing trend as those in Figs. 3(a) and 3(b), while those related to the unregulated graphene layer remain unchanged. Therefore, changing the Fermi energy, the working wavelengths of the polarization-sensitive multiband absorbers can be tuned actively, achieving a wide band regulation range of about 30 μm.

In addition, we also calculate the absorption spectra at different polarization angles to examin the dependence of the proposed structure on polarization angle. We set the polarization angle α to be 0° for the x polarization. It is obvious in Fig. 4(a) that the P_1 and P_2 weaken while the P_3 and P_4 strengthen with α increasing. For the polarization angle α of 45°, the electric field response in the x and y directions achieve dynamic balance, resulting in the four-mode state with the same strength. Extracting the maximum absorptions of the four peaks under different polarization angles, the results are shown in Fig. 4(b). The maximum absorptions of the peaks are all sensitive to polarization angle with a period of 180°. Therefore, both the peak number and the peak strength of the multiband absorber can be actively controlled by the polarization angle.

In order to illustrate the physical origin of the polarization-sensitive absorption, we calculate the electric field amplitude distributions of the structure under the x and y polarizations as displayed in Figs. 5 and 6, respectively. As shown in Figs. 5(a) and 5(c), the electric fields are strongly localized around the top graphene layer, while those around the bottom graphene are almost zero. The electric dipole modes excited in the top rectangular graphene and the aperture along the x direction forms the symmetric surface current along the x axis. Thus, peak P_1 mainly comes from the dipole modes excited in the top graphene layer and the aperture along the x direction. Similarly, as shown in Figs. 5(b) and 5(d), peak P_2 mainly results from the dipole modes excited around the bottom graphene rectanmgle. As a result, the two peaks in the x-direction can be independently excited, for there is nearly no field coupling between the top graphene and the bottom graphene at peaks P_1 and P_2.

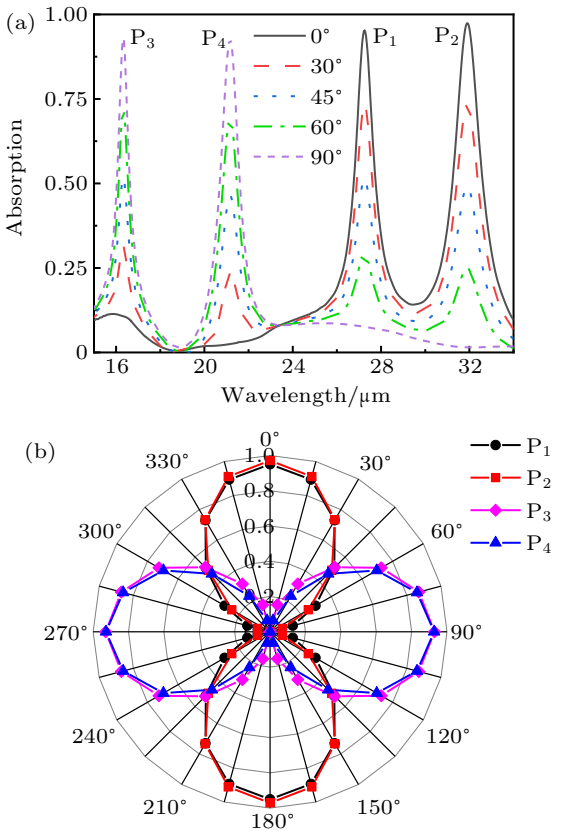


Fig. 4. (a) Absorption spectra under different polarization angles, and (b) maximum absorptions of peaks related to different polarization angles.

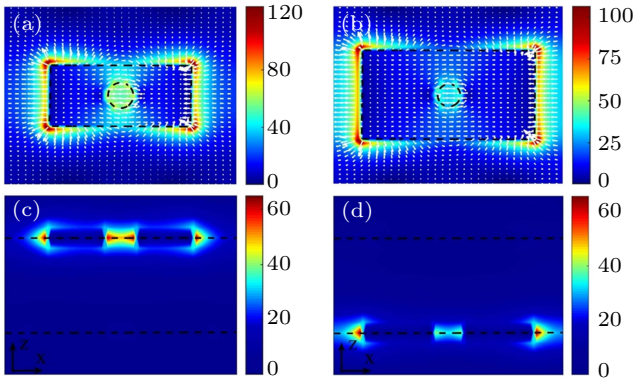


Fig. 5. Electric field amplitude and surface current distribution under x polarization, relating to [(a) and (c)] P_1 and [(b) and (d)] P_2. Panels (a) and (b) show electric field around the top and bottom graphene patches in x–y plane, while panels (c) and (d) display those in x–z plane, respectively. Black dashed lines indicate the place of graphene structures.

Under the y polarization, resonant modes around the graphene rectangle are also excited resulting in the absorption peaks P_3 and P_4. However, the length along the y direction is so short that there appears the coupling between the inner aperture and the outer rectangular, leading the field distributions to deform as shown in Figs. 6(a) and 6(b). As a result, the electric dipole-like field deforms into hexapole-like field distribution around the rectangle and the aperture, leading to the

symmetric surface current along the y axis. Like peaks P_1 and P_2, there is no field coupling effect between the two graphene layers at the absorption peaks P_3 and P_4 either. Therefore, the two absorption peaks in their own directions are independently determined by the graphene patches. Consequently, multiband absorption can be integrated into one structure by increasing the graphene layers.

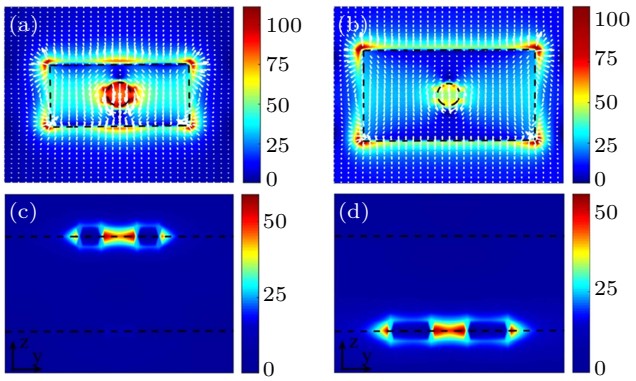


Fig. 6. Electric field amplitude and surface current distributions under y polarization at [(a) and (c)] P_3, [(b) and (d)] P_4. Panels (a) and (b) show electric field around the top and bottom graphene patches in x–y plane, while panels (c) and (d) display those in y–z plane, respectively.

In the above discussion above, there is almost no coupling between the two graphene layers. Next, we change thicknessd_1 of the silica layer to explore the influence on the coupling. For the x polarization, as d_1 decreases, the absorption peaks P_1 and P_2 shift toward different directions as shown in Fig. 7(a), with electric field increasing in the silica layer at the peaks as shown in Fig. 7(b), which suggests the increase of the coupling between the two graphene layers. For the y polarization shown in Fig. 7(c), the absorption peaks P_3 and P_4 shift to different directions as d_1 decreases, and meanwhile, the peak P_3 gradually splits into two peaks. According to the field distributions in Fig. 7(d), the hexapole-like mode relating to P_3 splits into a quadrupole-like mode ($\lambda = 15.4$ μm) and a dipole-like mode ($\lambda = 18.5$ μm) due to the coupling between the two graphene layers, resulting in the two peaks splitting from P_3. Therefore, the coupling between the two graphene layers strengthens as d_1 decreases under the x polarization and y polarization, which affects the wavelengths and the maxima of the absorption peaks. As a result, the thick silica layer is necessary to maintain the independent regulation properties of the multiband absorber.

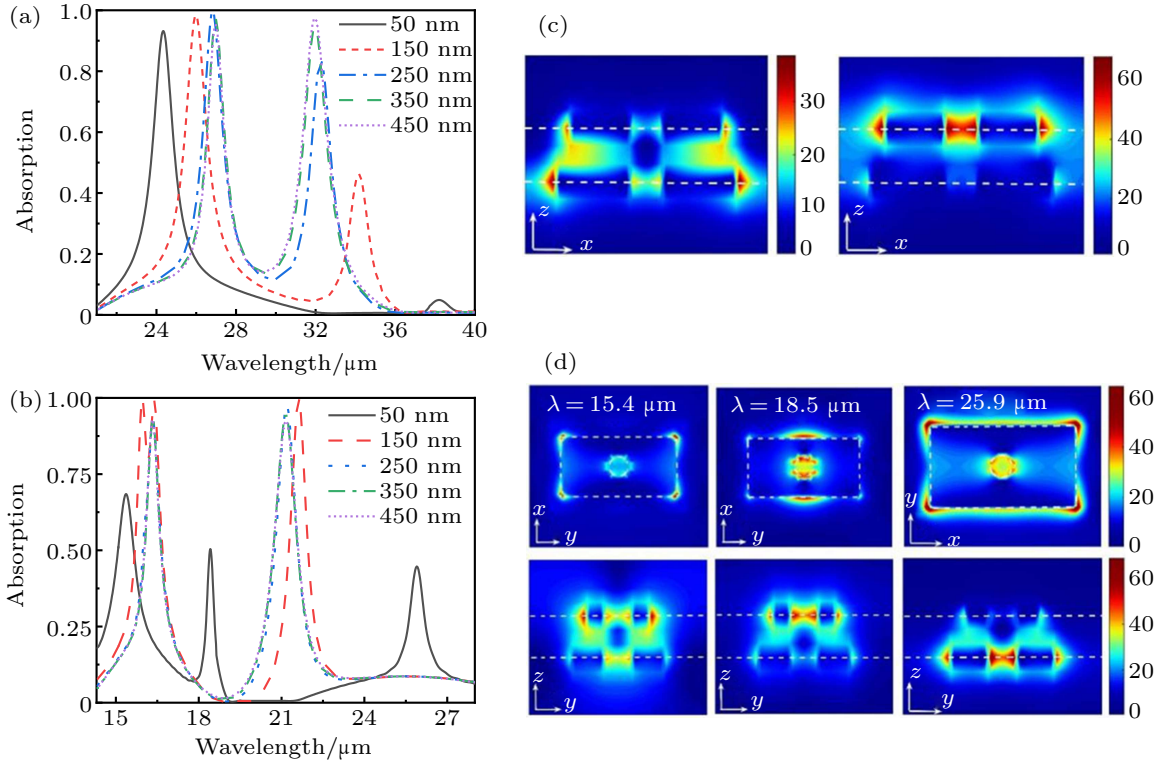


Fig. 7. (a) Absorption spectra for different values of d_1, (b) related electric field distributions under x polarization, (c) absorption spectra for different values of d_1, and (d) related electric field distributions undery polarization.

Based on the analyzation above, the absorption peaks can be affected by the geometric parameters of the graphene patches independently, so we change the top and bottom graphene layers to observe the specific effects on peaks P_1, P_2, P_3, and P_4. In Fig. 8(a), increasing the long side l_1 of the rectangular, the absorption peak P_1 is largely redshifted with the maximum absorption keeping constant, while the absorption peak P_3 is slightly blueshifted with the maximum absorption decreasing to below 90%. On the contrary, the absorption peak P_1 is slightly blue-shifted with the maximum absorption increasing as w_1 increases, while the absorption peak P_3 is largely red-shifted with the maximum absorption

fixed as shown in Fig. 8(b). Therefore, the length and width of the rectangle strongly shift the absorption peaks excited by the light polarized along the same direction, without affecting the amplitude, which also influences both the wavelength and the amplitude of the peak excited by the light polarized along the other directions. In Fig. 8(c), changing the diameter of the inner aperture, the absorption peaks P_1 and P_3 are both red-shifted. The maximum absorption relatively decreases under the x polarization, but increases under the y polarization. Similar variations happen to P_2 and P_4 when changing the parameters of the bottom graphene, which are shown in Figs. 8(d)–8(f), respectively. Consequently, the wavelength of the peak excited under the x polarization satisfies $\lambda_x \propto Dl/w$, under the y polarization it follows $\lambda_y \propto Dw/l$.

However, as the duty cycle of the aperture in the top layer is larger than that in the bottom layer, the resonance wavelength is more sensitive to the variety of parameter D_1 than that of parameter D_2.

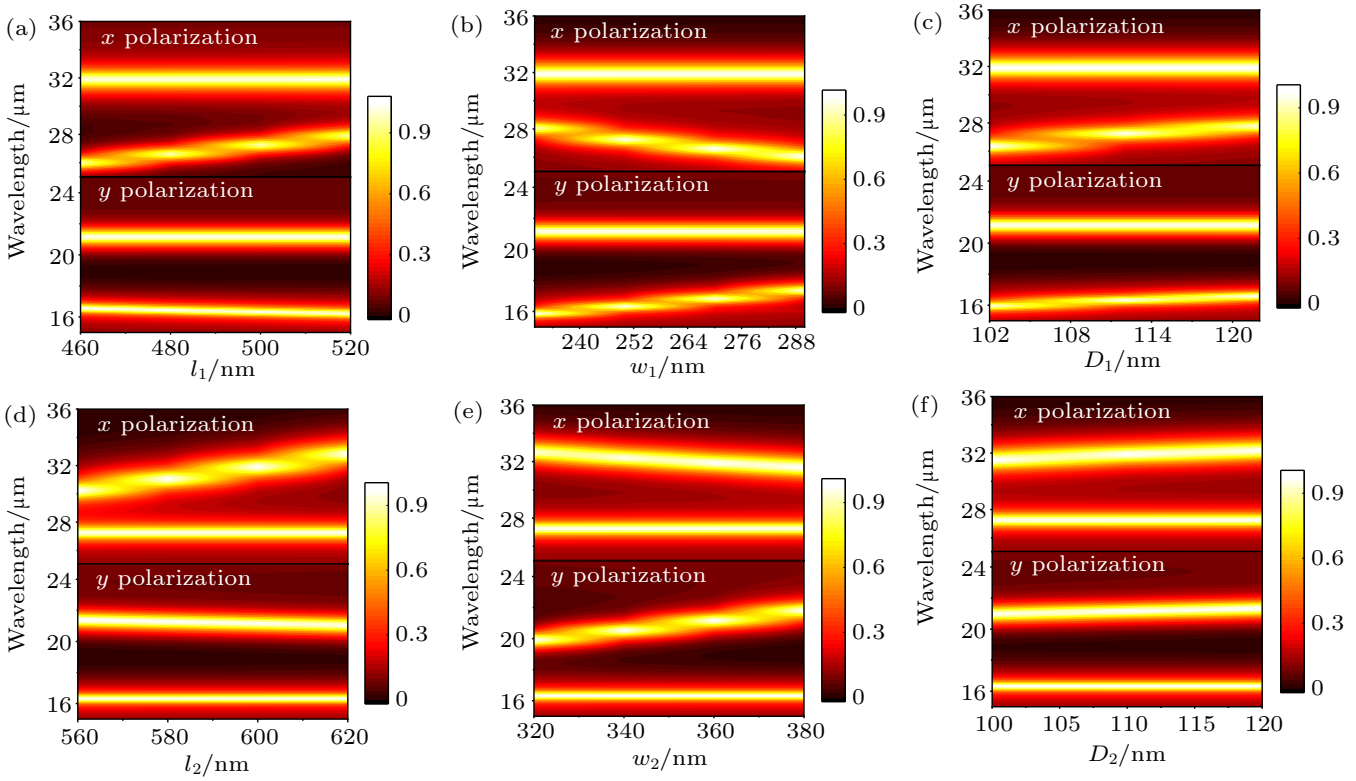


Fig. 8. Variations of absorption spectrum with (a) l_1, (b) w_1, (c) D_1, (d) l_2, (e) w_2, and (f) D_2, respectively.

4. Summary

To sum up, we have designed an actively tunable polarization-sensitive multiband absorber in the mid-infrared region. Combining the advantages of the graphene and anisotropic structure, the absorber shows distinct anisotropic plasmonic responses under different polarizations, resulting in dual-band absorption over 90%. Adjusting the Fermi energy of the graphene layer, the absorption band can realize dynamic regulation of extremely wide band. Besides, the peak number and the peak strength of the multiband absorber can be actively tuned by the polarization angle. As the absorption peak is excited in each graphene layer independently, more absorption bands can be achieved by increasing the graphene layers. We have proposed a method to design actively tunable polarization-sensitive multiband absorber, which may have potential applications in mid-infrared devices, such as filters and polarization detectors.

Acknowledgment

We thank Bingyu Chen and Yuyang Cheng for their help in simulations.

References

[1] Shelby R A, Smith D R and Schultz S 2001 *Science* **292** 77
[2] Jahani S and Jacob Z 2016 *Nat. Nanotechnol.* **11** 23
[3] Smith D R, Schultz S, Markos P and Soukoulis C M 2001 *Phys. Rev. B* **65** 195104
[4] Schurig D, Mock J J, Justice B J, Cummer S A, Pendry J B, Starr A F and Smith D R 2006 *Science* **314** 977
[5] Watts C M, Liu X and Padilla W J 2012 *Adv. Mater.* **24** OP98
[6] Liu X, Starr T, Starr A F and Padilla W J 2010 *Phys. Rev. Lett.* **104** 207403
[7] Landy N I, Sajuyigbe S, Mock J J, Smith D R and Padilla W J 2008 *Phys. Rev. Lett.* **100** 207402
[8] Liu N, Mesch M, Weiss T, Hentschel M and Giessen H 2010 *Nano Lett.* **10** 2342
[9] Katrodiya D, Jani C, Sorathiya V and Patel S K 2019 *Opt. Mater.* **89** 34
[10] Wu C H, Neuner B, Shvets G, John J, Milder A, Zollars B and Savoy S 2011 *Phys. Rev. B* **84** 075102
[11] Chen H T 2012 *Opt. Express* **20** 7165

[12] Zhu J F, Ma Z F, Sun W J, Ding F, He Q, Zhou L and Ma Y G 2014 *Appl. Phys. Lett.* **105** 021102
[13] Novoselov K S, Fal'ko V I, Colombo L, Gellert P R, Schwab M G and Kim K 2012 *Nature* **490** 192
[14] Geim A K and Novoselov K S 2007 *Nat. Mater.* **6** 183
[15] Novoselov K S, Jiang D, Schedin F, Booth T J, Khotkevich V V, Morozov S V and Geim A K 2005 *Proc. Natl. Acad. Sci. USA* **102** 10451
[16] Nikitin A Y, Guinea F, García-Vidal F J and Martín-Moreno L 2011 *Phys. Rev. B* **84** 161407
[17] Sun P, You C L, Mahigir A, Liu T T, Xia F, Kong W J, Veronis G, Dowling J P, Dong L F and Yun M J 2018 *Nanoscale* **10** 15564
[18] Fang Z Y, Wang Y M, Schlather A E, Liu Z, Ajayan P M, de Abajo F J G, Nordlander P, Zhu X and Halas N J 2014 *Nano Lett.* **14** 299
[19] Huang M L, Cheng Y Z, Cheng Z Z, Chen H R, Mao X S and Gong R Z 2018 *Opt. Commun.* **415** 194
[20] Ke S L, Wang B, Huang H, Long H, Wang K and Lu P X 2015 *Opt. Express* **23** 8888
[21] Bao Z Y, Wang J C, Hu Z D, Balmakou A, Khakhomov S, Tang Y and Zhang C L 2019 *Opt. Express* **27** 31435
[22] Hu J, Liu W, Xie W, Zhang W, Yao E, Zhang Y and Zhan Q 2019 *Opt. Lett.* **44** 5642
[23] Yao G, Ling F, Yue J, Luo C, Ji J and Yao J 2016 *Opt. Express* **24** 1518
[24] Hu J, Yao E, Xie W, Liu W and Zhan Q 2019 *Opt. Express* **27** 18642
[25] Fan C, Tian Y, Ren P and Jia W 2019 *Chin. Phys. B* **28** 076105
[26] Wang J, Gao C N, Jiang Y N and Akwuruoha C N 2017 *Chin. Phys. B* **26** 114102
[27] Wang L, Ge S J, Hu W, Nakajima M and Lu Y Q 2017 *Opt. Express* **25** 23873
[28] Xia Y Y, Dai Y, Wang B, Chen A, Zhang Y B, Zhang Y W, Guan F, Liu X H, Shi L and Zi J 2019 *Opt. Express* **27** 1080
[29] Cai Y J and Xu K D 2018 *Opt. Express* **26** 31693
[30] Zhang J F, Zhu Z H, Liu W, Yuan X D and Qin S Q 2015 *Nanoscale* **7** 13530
[31] Piper J R and Fan S H 2014 *ACS Photon.* **1** 347
[32] Bao Q L, Zhang H, Wang B, Ni Z H, Lim C H Y X, Wang Y, Tang D Y and Loh K P 2011 *Nat. Photon.* **5** 411
[33] Hanson G W 2008 *J. Appl. Phys.* **103** 064302
[34] Li K, Xia F, Wang M, Sun P, Liu T, Hu W P, Kong W J, Yun M J and Dong L F 2017 *Carbon* **118** 192
[35] Hanson G W 2008 *J. Appl. Phys.* **104** 084314
[36] Koppens F H L, Chang D E and de Abajo F J G 2011 *Nano Lett.* **11** 3370
[37] Novoselov K S, Geim A K, Morozov S V, Jiang D, Zhang Y, Dubonos S V, Grigorieva I V and Firsov A A 2004 *Science* **306** 666
[38] Gómez-Díaz J S and Perruisseau-Carrier J 2013 *Opt. Express* **21** 15490